Numerical analysis of the effect of tire characteristics, soil response and suspensions tuning on the comfort of an agricultural vehicle

S. Melzi *, S. Negrini, E. Sabbioni

Dipartimento di Meccanica, Politecnico di Milano, via La Masa 1, 20156 Milan, Italy

Received 17 December 2013; received in revised form 18 March 2014; accepted 15 May 2014

1. Introduction

Agricultural tractors have to accomplish a multiplicity of different missions: they should develop high thrusts on deformable soils, they could be used for road and off-road transportation, they should guarantee adequate speed and handling performance on ordinary roads and they should provide good comfort levels. This last aspect is related to the vibration induced on the vehicle chassis by irregularity and deformation of the track and by the use of lugged tires [1]. Due to the continuous increase of tractors speed, issues relevant to comfort levels are becoming critical especially for their impact on riding safety. In fact, besides undermining operator's health on a long-time base [1–3], the exposure to high vibration levels affects the efficiency and the alertness of the operator [4–6], thus leading to unsafe operating conditions. Considering that the rear axle of tractors is often unsuspended and suspensions on the front axle are usually locked during field operation, other suspension levels are introduced to guarantee adequate riding comfort. The first suspension level is represented by radial flexibility of tires. The second level is located between the chassis and the tractor cabin while the driver seat, which is often suspended, constitutes the last level.

This work analyzes the comfort levels of a tractor during field operation from a numerical point of view. The aim of the analysis is to determine the optimal combination of suspension parameters which leads to minimize the acceleration levels transmitted to the operator. The model used in the numerical analysis combines a multi-body model of tractor and a tire–soil interaction model. The tractor model consists of a lumped parameters model whose data were identified through a series of tests carried out with a four-post test bench [7,8]. The tire–soil interaction model

* Corresponding author. Tel.: +39 0223998458.
E-mail address: stefano.melzi@polimi.it (S. Melzi).

allows the computation of the contact forces developed by a lugged tire operating on a deformable soil; the model takes into account the 3D geometry of the tread surface and the main mechanical characteristics of the soil. Thus, the proposed model includes the most important factors influencing riding comfort: terrain deformation, tread pattern design, tire flexibility and suspensions characteristics. Also soil irregularity was considered.

Simulations were carried out assuming a tractor moving at 7 km/h over a deformable soil; several combinations of suspensions parameters were tested in order to evaluate the improvement with respect to nominal settings. The analysis was repeated with four scenarios combining two tires with different size and tread pattern with two terrains with different mechanical responses.

The paper is organized as follows: the first section is focused on the multi-body model of the tractor; the second part of the article deals with the tire–soil interaction model. The last section presents the numerical analysis aiming at optimizing the suspensions parameters.

2. Multi-body model of the vehicle

The modeled agricultural tractor is a high-range tractor, whose mass and main dimensions are reported in Table 1.

The tractor is composed of a frame (vehicle body) on which are placed the engine and the cabin. The cabin is connected to the frame by means of three passive pneumatic suspensions (air springs). Independent actively controllable double wishbone suspensions join the front tires with the frame. A pair of electronically controlled hydropneumatic actuators allow to regulate the length of the suspensions. Two working conditions are supported by the suspension system: during field operations (tilling, ground compaction, etc.), the actuators can be locked up (the suspension is thus rigid) in order to increase traction, whereas, when the vehicle is running on ordinary roads, the actuators can be unlocked in order to damp vehicle pitch. The front suspension can be manually switched on or off by the operator. On the contrary, no suspensions are present between the rear axle and the frame. Finally a pneumatic spring and a damper connect the seat with the cabin.

A sketch of the proposed tractor model is presented in Fig. 1; the model is made up of several rigid bodies linked by linear spring-damper elements:

- one rigid body representing the vehicle chassis having three d.o.f. (heave, pitch and roll); this body includes the rear axle, which is assumed to be rigidly linked to the chassis;

Table 1
Vehicle mass and geometry.

Total mass	[kg]	10,320
Wheelbase	[m]	3.06
Front track	[m]	2.11
Rear track	[m]	2.01

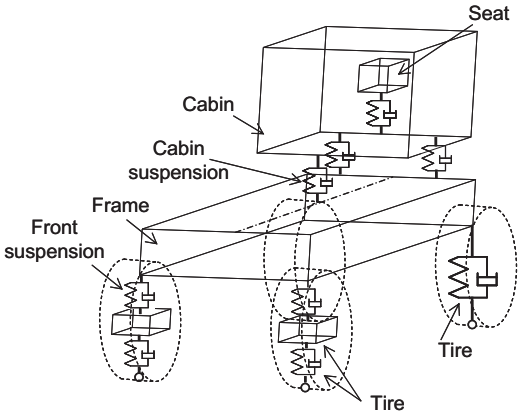

Fig. 1. MB vehicle model.

- one rigid body representing the cabin, characterized by three d.o.f. (heave, pitch and roll);
- two rigid bodies representing the front unsprung masses (the examined vehicle presents independent front suspensions), each one having one d.o.f. (heave);
- one rigid body having one d.o.f (heave), representing the seat and the load mounted on it which simulates the equivalent mass of the operator;
- four rigid rings representing the outer part of the four tires (the part contacting the ground); each ring presents a vertical motion and a rotation along the hub.

Spring-damper elements represent the front suspension of the chassis and the suspension system of cabin and of the seat; the rigid ring of each tire is connected to the corresponding hub through spring-damper elements which represent the front and rear tires vertical stiffness and damping.

2.1. Parameters identification and model validation

Several experimental tests were performed on the examined tractor with the purpose of identifying the parameters of the multi-body model and to obtain a validation of the model itself. During the tests, the vehicle was instrumented with

- four one-axis piezoelectric accelerometers placed in correspondence of each hub to measure their vertical accelerations;
- four one-axis piezoelectric accelerometers placed in correspondence of each attachment point of the suspensions on the chassis;
- an inertial gyroscopic platform in order to measure the accelerations of the cabin along the three axes of motion (longitudinal, x, lateral, y, and vertical, z) and the angular velocities of pitch (rotation about axis y: ω_y), roll (rotation about axis x: ω_x) and yaw (rotation about axis z: ω_z);
- two three-axis piezoelectric accelerometers placed in correspondence of the seat plane and of the back support in order to evaluate the operator comfort;

- four one-axis piezoelectric accelerometers in order to measure the four-post test-rig actuator pads acceleration (input of the system).

All the signals were acquired with a sample frequency of 500 Hz and low-pass filtered at 15 Hz.

Experimental tests were performed using a four poster test rig, specifically designed to test big and heavy vehicles with a weight up to 15 tons. Tests have been performed imposing chirp signals (sweep sine tests) to the four-post test rig pads and random excitations in the frequency range 0–20 Hz [7,8]. Sweep sine tests have been carried out in order to excite the vehicle eigenmodes of heave, roll and pitch separately. In order to excite the vertical motion of the vehicle, the four actuators of the test-rig have been moved in phase. By moving the rear actuators in counter phase with respect of the front ones, the pitch motion has been evaluated. Finally, moving the right actuators in counter phase with respect of the left ones, the roll motion has been excited. Tests have been repeated considering different excitation amplitudes, different tire pressures and with the front suspension switched off and on.

Data collected with sweep sine tests were used to identify multi-body viscoelastic parameters. Test conditions were reproduced in the virtual environment and viscoelastic parameters were tuned so that the frequency response of the model could match the experimental one. Figs. 2 and 3 report comparison between model response and experimental data referring to a sweep sine test with all the actuators moved in phase and to a sweep sine test with the front actuators moved in counter phase with respect to the rear ones. During the tests the front suspension system was switched off. Figs. 4 and 5 refer to the same test performed with front suspensions unlocked. The transfer functions (TF) between the rear right pad acceleration and the cabin heave and pitch accelerations are shown. The model results are represented with black lines, while the experimental data by the red dashed lines. A good agreement can be noticed between the experimental and the model results, both for the amplitude and the phase of the TFs.

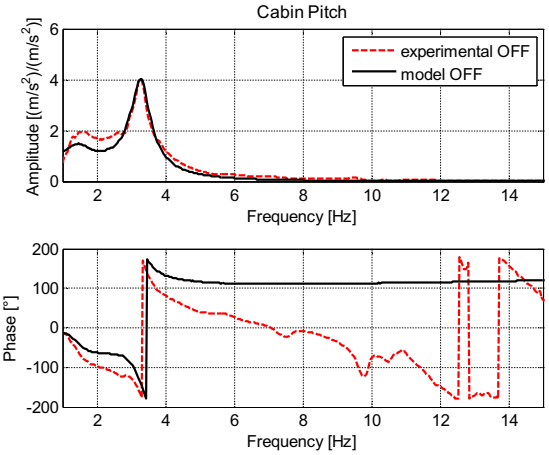

Fig. 3. Numerical-experimental comparison: cabin pitch accelerations during a sweep sine test with front and rear actuators moved in counter phase. Front suspensions locked.

Identified model parameters are listed in Table 2.

The second session of experimental tests, i.e. random tests, aimed at reproducing the operating condition of a tractor running on agricultural soil. For the purpose, time histories of the acceleration on the four hubs were recorded during an outdoor test-session with the tractor moving on deformable soil; four-post actuators were then driven to reproduce the same time histories on the four hubs during an indoor test section. In this way the test bench was used to simulate on-field operation where tire–soil interaction actually gives rise to a random excitation which excites all the rigid modes of the vehicle. Data of this test were thus used for model validation. Fig. 6 shows comparisons between experimental data and model outputs in terms of

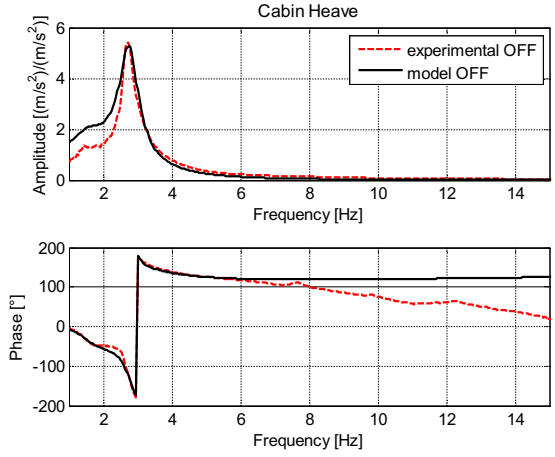

Fig. 2. Numerical-experimental comparison: cabin heave accelerations during a sweep sine test with all the actuators moved in phase. Front suspensions locked.

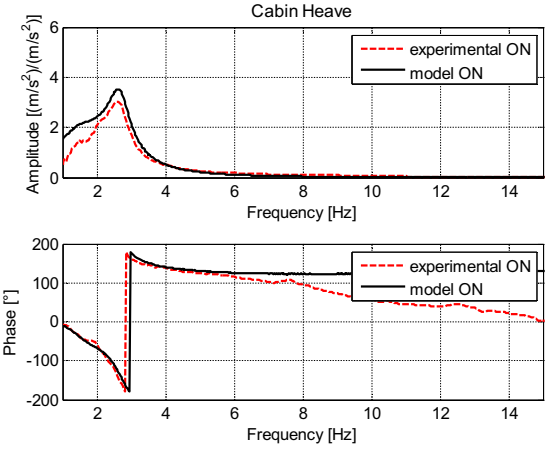

Fig. 4. Numerical-experimental comparison: cabin heave accelerations during a sweep sine test with all the actuators moved in phase. Front suspension unlocked.

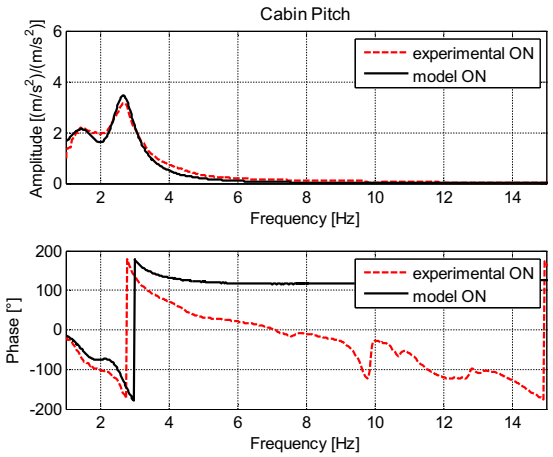

Fig. 5. Numerical-experimental comparison: cabin pitch accelerations during a sweep sine test with front and rear actuators moved in counter phase. Front suspension unlocked.

Table 2
Model stiffness and damping.

Visco-elastic element	Stiffness (N/m)	Damping (Ns/m)
Frame suspensions		
Front	320,000	40,000
Rear	–	–
Cabin suspensions		
Front	73,724	5000
Rear	73,724	5000
Seat suspensions	5840	624
Tire		
Front	628,470	4902
Rear	699,512	4482

vertical acceleration on driver seat, cabin center of gravity, right front and right rear hub. Both time histories and spectra are compared. In general a good agreement is observed in particular as far as seat and cabin acceleration is concerned; these signals can be regarded as the most important for comfort evaluation.

3. Tire-soil numerical model

Tire-soil numerical model allows computation of the forces developed at the contact interface while a lugged tire interacts with a deformable soil. The model considers the dynamics of the tire in the vertical plane and takes into account the 3D geometry of the tread pattern.

3.1. Soil model

The soil has been schematized as a continuous layer of springs whose compression, caused by the sinking of the tire, produces a normal contact stress. The contact stress is assumed to be hydrostatic and the relation between sinking z and normal stress σ is not univocal but depends on the time history of the deformation. In particular, as shown in Fig. 7, different slopes in the z–σ relation are assumed when considering the first soil deformation and when considering repeated compressions or deformation recovery. This model allows estimation of the permanent deformation of the soil associated with the tire passage.

The Mohr–Coulomb failure criterion [9] is applied to determine the maximum tangential stress sustained by the soil:

$$\tau_{max} = c + \sigma \tan \varphi \tag{1}$$

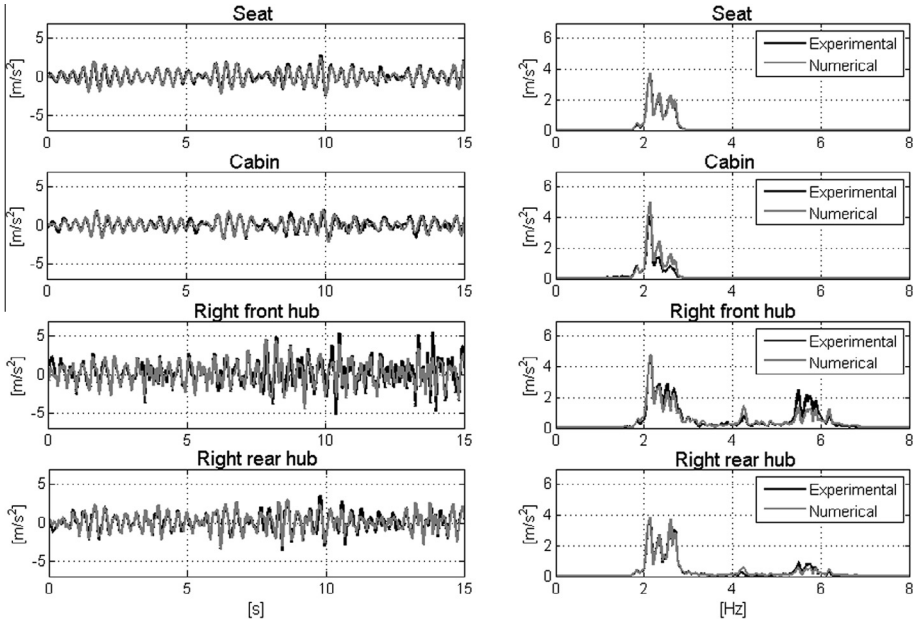

Fig. 6. Random tests, numerical-experimental comparison in terms of vertical acceleration on driver seat, cabin c.o.g., right front hub and right rear hub.

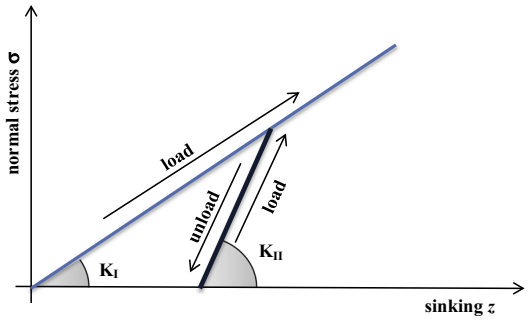

Fig. 7. Scheme of the relationship between sinking and hydrostatic normal stress in the soil; the slope of the initial load curve is equal to K_I while the slope of the unload curve is equal to K_{II}.

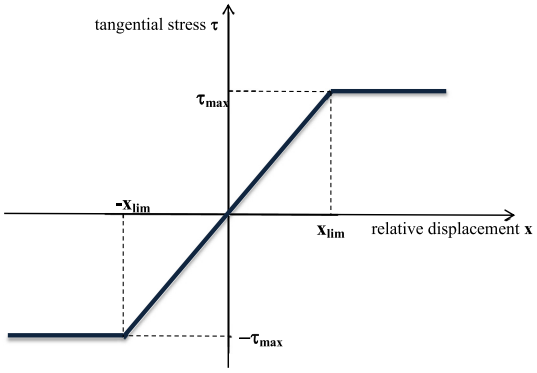

Fig. 8. Relationship between relative tangential displacement between tire and soil and the tangential stress.

where c is the cohesion and φ is the free angle of shearing resistance. The tangential contact stress developed at the tire-terrain interface is computed considering the relative tangential displacement between the layer of soil directly in contact with the tire and the undeformed terrain. The tangential stress τ increases linearly with the relative displacement between the layers of soil, until the value τ_{max} is reached (see Fig. 8).

The maximum tangential stress developed by the soil is reached for a given relative displacement x_{lim} that is a property of the considered soil. Once the maximum allowable value τ_{max} is reached, the tangential stress is kept constant and equal to the limit value τ_{max} until the contact between soil and tread element is abandoned. This behavior conveniently reproduces the response of a plastic terrain.

3.2. Tire model

The tire is schematized through a rigid ring representing the tire carcass; this last is linked to the tire hub by means of a spring-damper element which describers the carcass flexibility along the radial direction. The motion of the tire is assumed to take place in the vertical plane, thus 2D dynamics are considered.

The 3D geometry of the tread pattern is introduced in the model with the following procedure; as shown in Fig. 9, the tread surface is divided into a series of elements. Each element of the grid is characterized with the area of

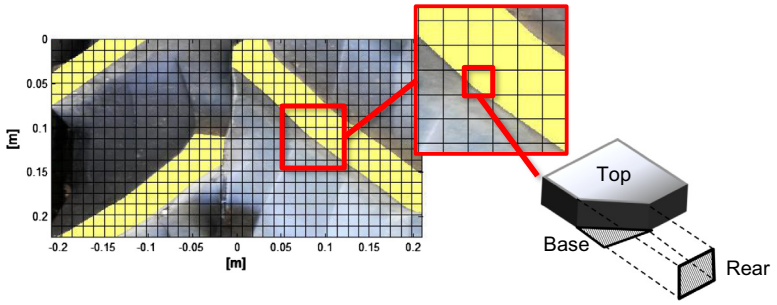

Fig. 9. Gridding of the tire rolling surface through a uniform rectangular grid.

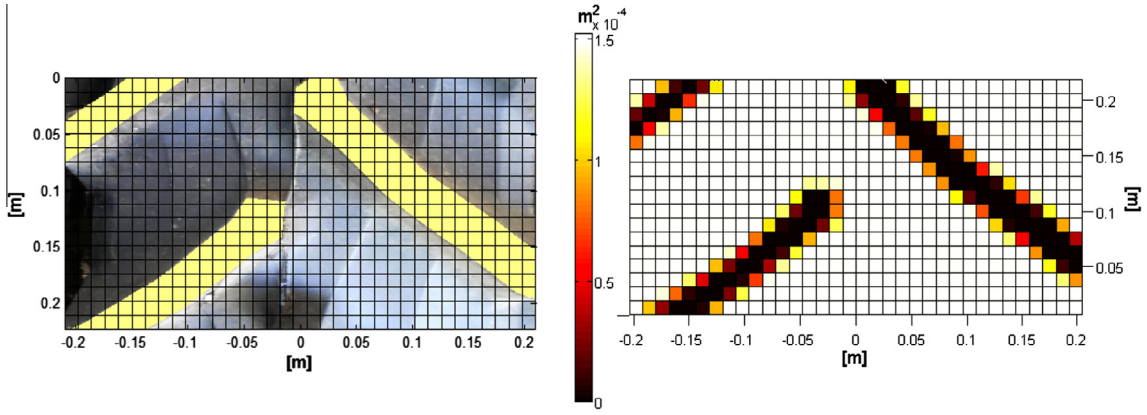

Fig. 10. Base surface [m^2] for each grid element. for a 12 × 12 mm grid.

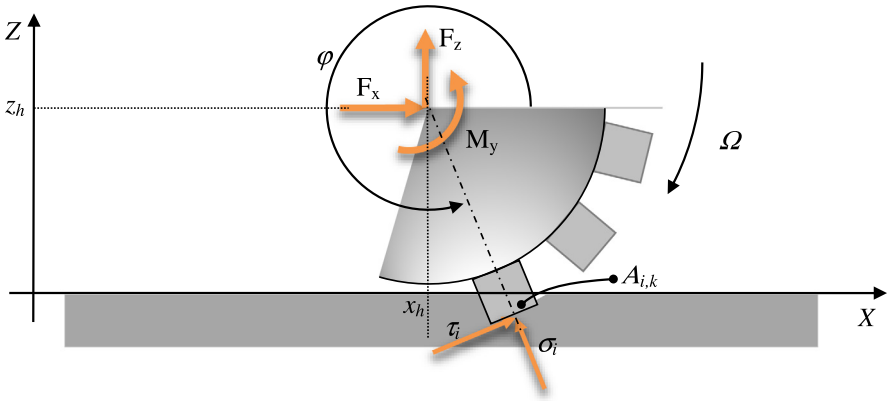

Fig. 11. Local and global contact forces.

four surfaces named: *top*, *base*, *front and rear*. Top surfaces represent the outer part of the tread lugs; base surfaces represent the area between lugs; front and rear surfaces represent the lugs sides. Each element of the grid is assumed to exchange normal and tangential forces through these surfaces. For example, grid elements between lugs are able to exchange forces only through the base, grid elements on top of the lugs are able to exchange forces only through top surface, while grid elements positioned across the lug sides, are able to exchange forces both through the top/base and the front/rear surfaces.

Fig. 10 shows the values of base surfaces for each grid element. Each surface of each grid element is also characterized with a geometrical center, whose position and speed are used to compute the sinking and the relative speed with respect to the soil.

3.3. Tire soil interaction

As discussed before, the tread surface is discretized into several elements, each one exchanging normal and tangential forces with the ground through 4 surfaces; the relative speed of the center of a tread element with respect to the soil is projected along a direction tangent to the contact surface and its integration allows to determine the relative tangential displacement used to compute the tangential stress according to Eq. (1) and to the scheme of Fig. 8.

The soil itself is discretized with a number of elements each one presenting a different history of previous deformations. The grid adopted to discretize the terrain does not in general conform with the one used for the tread surface, so a linear interpolation is implemented to compute the deformation of the soil (in vertical direction) associated with the position of a tread element.

The longitudinal and vertical contact forces (F_x and F_z) and the torque M_y are obtained by adding the contributions of normal and tangential forces acting on each element and projecting them along the global longitudinal and vertical directions; making reference to Fig. 11, the contact forces are thus given by:

$$\begin{cases} F_x = -\sum_{i=1}^{N}\sum_{k=1}^{4}\left[\sigma_{i,k}\cos\varphi_{i,k} + \tau_{i,k}\sin\varphi_{i,k}\right]A_{i,k} \\ F_z = \sum_{i=1}^{N}\sum_{k=1}^{4}\left[-\sigma_{i,k}\sin\varphi_{i,k} + \tau_{i,k}\cos\varphi_{i,k}\right]A_{i,k_i} \\ M_y = \sum_{i=1}^{N}\sum_{k=1}^{4}\left[-\sigma_{i,k}\sin\varphi_{i,k} + \tau_{i,k}\cos\varphi_{i,k}\right]A_{i,k}\cdot(x_{i,k}-x_h) \\ \quad +\left[\sigma_{i,k}\cos\varphi_{i,k} + \tau_{i,k}\sin\varphi_{i,k}\right]A_{i,k}\cdot(z_{i,k}-z_h) \end{cases} \tag{2}$$

In (2) $\sigma_{i,k}$ and $\tau_{i,k}$ respectively represent the normal and tangential stress acting on the kth surface of ith tread element; as described before, each element presents four surfaces (base, top, front and rear) where interaction between soil and tire takes place. $A_{i,k}$ is the area of the kth surface, while $\varphi_{i,k}$ identifies the angular position of the vector normal to the surface and outward facing. Considering the computation of torque M_y, $x_{i,k}$ and $z_{i,k}$ define the horizontal and vertical position of the geometrical center of $A_{i,k}$ with respect to a global reference X–Z, while x_h and z_h define the position of the tire hub.

4. Numerical analysis

The model presented above was used to investigate the influence of suspensions damping on driver comfort. In particular, the effect of damping of front axle, cabin and seat were considered. Different configurations were compared in terms of RMS value of vertical acceleration on driver seat. During each simulation the tractor was assumed to run at a speed of 7 km/h over an undeformed soil with a tire slippage of 30%; this speed is typical for tillage operations, while the value of slippage is usually closer to the maximum traction force provided. The soil irregularity has been generated from a PSD built on the basis of data collected in a previous experimental campaign [10].

Four scenarios were analyzed, considering the tractor equipped with two different sets of tires and operating over two different soils. The main characteristics of the tires are

Table 3
Tires characteristics.

Tire	Size	Number of tread lugs (per side)	Tread lugs mean height (mm)	Max lugs angle (°)
TA	540/65R28	20	44.1	45
TB	420/70R30	19	43.6	45

Fig. 12. Treads shape of tire TA.

Fig. 13. Treads shape of tire TB.

listed in Table 3: tire TA is 540 mm wide, whereas tire TB is narrower (420 mm wide). Moreover tire TA presents a larger number of higher tread lugs (see Figs. 12 and 13). Distance between consecutive lugs of the same side is approximately 0.22 m for both the tires.

The characteristics of the soil have been drawn from technical literature, where many different soils are classified according to their Bekker's parameters [9,11]. The well known relationship between the normal pressure σ and the sinking z is reported in Eq. (3), where b is the tire width.

$$\sigma = (k_c/b + k_\phi)z^n \tag{3}$$

Table 4
Soils characteristics.

Soil	k_c (kN/m^{n+1})	k_φ (kN/m^{n+2})	n	c	φ
North Gower loam (NGL)	41.6	2471	0.73	6.1	26.6
Upland sandy loam (USL)	65.5	1418	0.97	3.3	33.7

The soils considered are named North Gower loam (NGL) and Upland sandy loam (USL): NGL is the harder soil whereas USL is the softer one, as it is possible to infer from their parameters listed in Table 4. As far as the parameter x_{lim}, used in the tangential stress model, is concerned, its value was set to 5 mm.

Combining Eq. (3) with the geometrical parameters of tires TA and TB and neglecting the effect of tread lugs (i.e. assuming a slick tire with the same dimensions), the relation between normal contact force and tire sinking can be carried out. Data collected in Table 5 show the sinking and the equivalent contact stiffness computed according to Bekker's formulation, considering the rear tire loaded with 32 kN. NGL clearly reveals a stiffer response; in addition, when the same terrain and the same sinking are considered, a higher normal contact force is developed on tire TA due to the increased width. Altogether, four different values of contact stiffness are obtained when coupling the two tires with the two soils. When operating on both harder (NGL) and softer (USL) terrain the contact stiffness is comparable to the vertical (radial) stiffness of the tire alone (Table 2) and, therefore, plays a role in affecting comfort levels.

4.1. Seat and cabin suspensions influence

During machinery operations the tractor front suspensions are locked in order to guarantee an improved control on tractive force [12]; hence, in a first series of simulations, the influence of cabin and seat damping on comfort was investigated assuming that both front and rear axle are rigidly linked to the tractor chassis. A second series of numerical analysis, reported in the next paragraph, was instead focused on the possibility of unlocking the front axle and thus exploiting an additional suspension level.

Figs. 14–17 show the trend of the standard deviation of vertical acceleration on the driver seat as a function of cabin and seat damping. Each figure refers to a different combination of soil and tire characteristics: Figs. 14 and 15 display results of simulations on NGL with tire A and tire B respectively; Figs. 16 and 17 present the results of simulations on USL.

Considering the data collected in Table 2, nominal values for suspension damping are 5000 Ns/m and 624 Ns/m for cabin and seat respectively. Besides the differences in absolute values, for all the examined scenarios, increasing cabin damping lowers the standard deviation of the seat vertical acceleration, until an asymptote is reached. For cabin damping higher than 15,000 Ns/m (3 times the nominal value), the standard deviation decreases less than 1%. Moreover, as far as seat damping effect is concerned, it is possible to observe that for values beyond 2496 Ns/m (i.e. 4 times the nominal value), seat acceleration levels become asymptotic and are no longer significantly affected by this parameter.

From the results of these simulations it is possible to infer that for seat damping of 2496 Nm/s and cabin

Table 5
Sinking and equivalent contact stiffness for the rear tire; values estimated according to Bekker formulation.

Soil	Tire	Estimated sinking (m)	Equivalent contact stiffness (N/m)
North Gower loam	TA	0.024	1.70e6
	TB	0.030	1.36e6
Upland sandy loam	TA	0.063	0.77e6
	TB	0.075	0.65e6

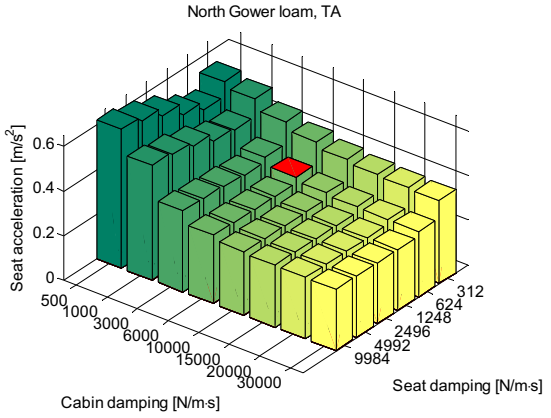

Fig. 14. RMS of seat vertical acceleration. Soil NGL, tire TA. Nominal conditions are marked in red. (For interpretation of the references to colour in this figure legend, the reader is referred to the web version of this article.)

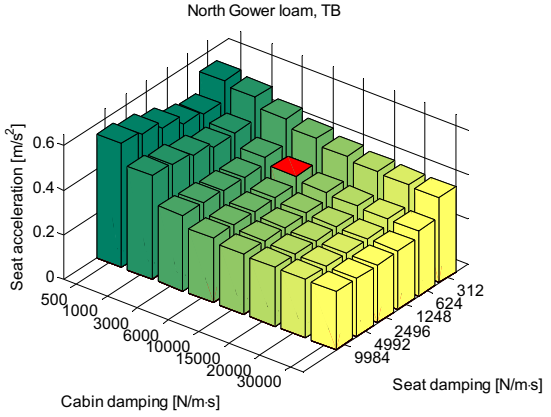

Fig. 15. RMS of seat vertical acceleration. Soil NGL, tire TB. Nominal conditions are marked in red. (For interpretation of the references to colour in this figure legend, the reader is referred to the web version of this article.)

damping of 15,000 Ns/m the minimum value of the seat acceleration standard deviation can be considered reached. According to numerical simulation, these values lead to minimize vertical acceleration on driver seat with all the combinations of tires and terrains considered.

Table 6 compares the RMS values of vertical acceleration on the seat estimated for a vehicle with nominal and optimized suspensions. It is possible to observe how RMS values can be reduced approximately by 18% on

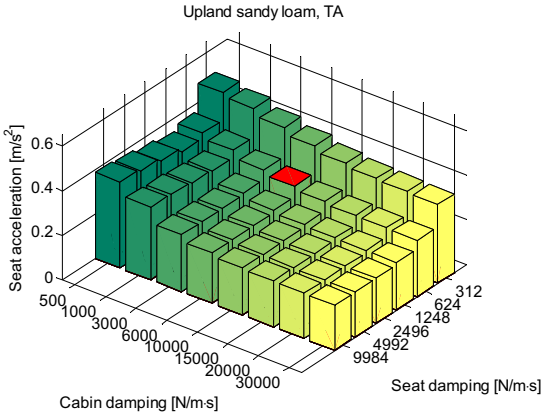

Fig. 16. RMS of seat vertical acceleration. Soil USL, tire TA. Nominal conditions are marked in red. (For interpretation of the references to colour in this figure legend, the reader is referred to the web version of this article.)

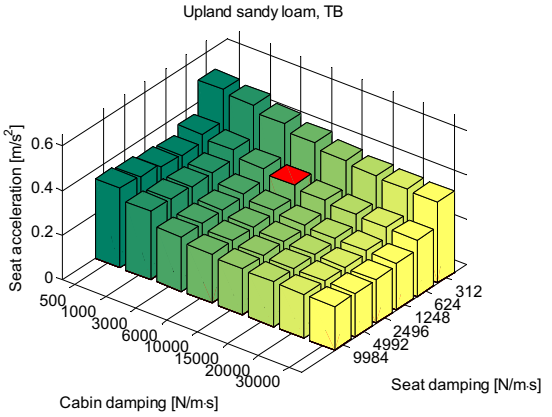

Fig. 17. RMS of seat vertical acceleration. Soil USL, tire TB. Nominal conditions are marked in red. (For interpretation of the references to colour in this figure legend, the reader is referred to the web version of this article.)

NGL and by 28% on USL with an appropriate combination of seat and cabin damping. It is noteworthy that RMS values obtained on NGL are markedly higher with respect to those obtained on USL; when considering the optimized suspensions, RMS values on NGL are nearly 30% higher than the ones on USL. The different characteristics of the tires analyzed in this work reveal instead a limited effect on comfort levels. In particular the narrower tire allows a decrease of RMS values around 5% with respect to the wider one for the optimum configuration, whereas very little influence is observed for the nominal configuration. In total, acceleration levels in optimal configuration appear almost scaled according to the equivalent vertical stiffness at the contact interface, which depends both on soil and tire characteristics (Table 5).

The comparison between Figs. 18 and 19 clearly reveals how soil stiffness influences tire sinking. Each picture shows the permanent deformation of the soil associated with the passage of the tractor; Fig. 18 refers to tire TA on NGL

Table 6
RMS of vertical acceleration in nominal and optimum configurations.

Soil	Tire	Nominal (m/s^2)	Optimum (m/s^2)	Improvement (%)
North Gower loam	TA	0.327	0.275	16
	TB	0.326	0.262	20
Upland sandy loam	TA	0.285	0.208	27
	TB	0.288	0.201	30

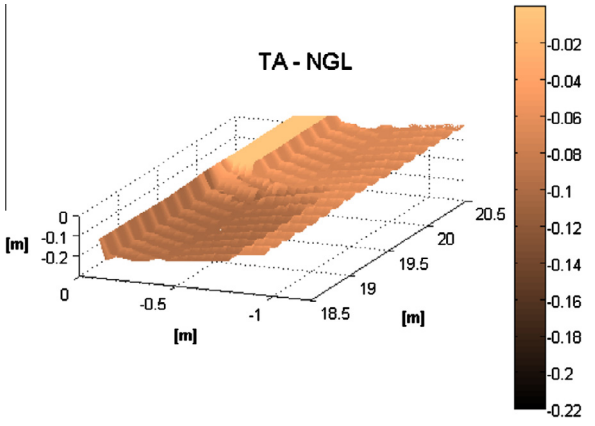

Fig. 18. Soil sinking after tractor passage, optimum damping configuration; soil NGL, tire TA.

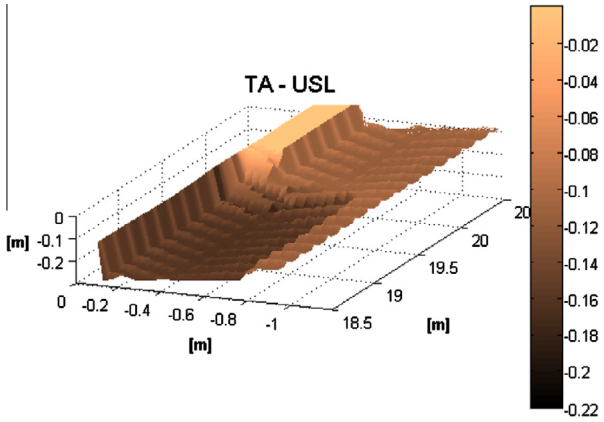

Fig. 19. Soil sinking after tractor passage, optimum damping configuration, soil USL, tire TA.

(the harder soil), while Fig. 19 is relevant to the same tire on USL. The left part of each figure presents a deeper compression due to the passage of the rear tire whose grooves are partially superposed to the ones of the front tire; the right part of each figure put into evidence the compression produced by the front tire and a portion of undeformed soil. The maximum depth of the grooves for the rear tire is around 0.09 m and 0.17 m for NGL and USL respectively. Values are higher with respect to those reported in Table 5, due to the previous compression generated by the front tire and to the non uniform distribution of contact pressure of the lugged tire.

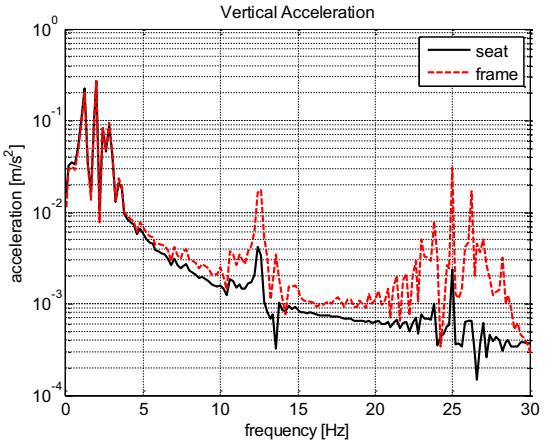

Fig. 20. Vertical acceleration as a function of the frequency; comparison between seat and frame, optimal configuration of dampers. Terrain north Gower loam, tire A.

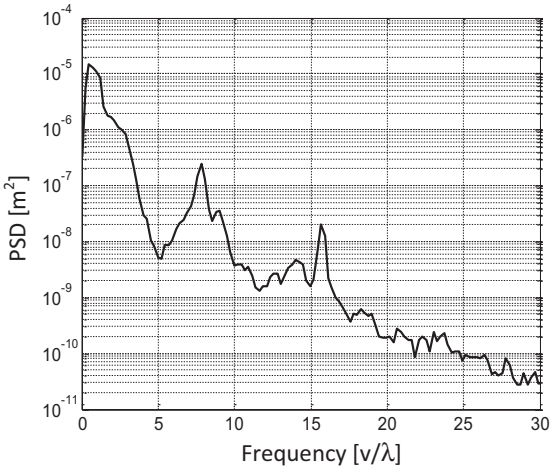

Fig. 21. Soil power spectral density (PSD).

The analysis of Fig. 20 allows quantification of the contribution of various harmonic components to vertical acceleration estimated on driver seat. Fig. 20 refers to the vehicle operating on NGL (the harder soil) equipped with a set of tires TA; spectra of vertical acceleration on the frame and on the seat are shown in semi-logarithmic scale. It is clearly possible to observe the role of the suspensions in filtering out the higher harmonic components of frame vertical acceleration. In particular, the effect of tread lugs is represented by peaks around 12 and 25 Hz. These two contributions are associated with the number of lugs per side and with the total number of lugs.

Besides a little contribution resulting from the contact between lugs and soil, most part of the vertical acceleration on the seat is due to low frequency modes. The first part of the spectrum presents a peak at 1 Hz associated with the seat resonance and two peaks at 2 and 2.5 Hz associated with cabin heave and pitch respectively. At low frequencies, the amplitude of seat acceleration is comparable with the

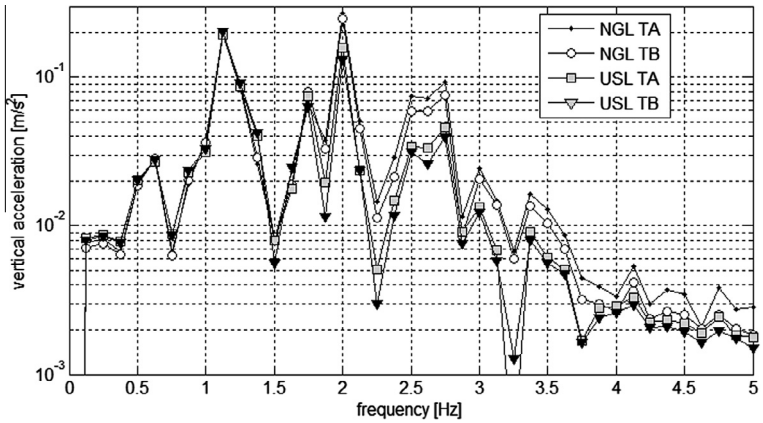

Fig. 22. Seat vertical acceleration as a function of the frequency; optimal configuration of dampers for four different combination of soil and tires.

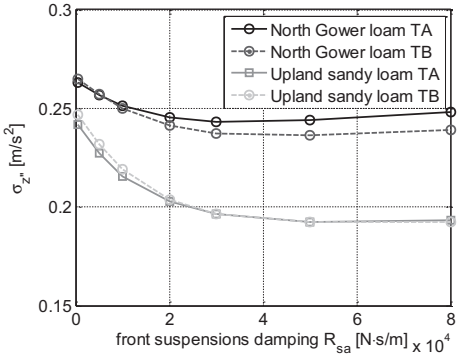

Fig. 23. Standard deviation of the vertical acceleration of the seat, as a function of front suspensions damping.

Table 7
Optimum configurations as a function of front suspensions damping.

Soil	Tire	Front suspensions damping (Ns/m)	RMS of seat vertical acceleration (m/s^2)	Improvement (%)
North Gower loam	TA	30,000	0.243	12
	TB	50,000	0.236	11
Upland sandy loam	TA	50,000	0.192	7
	TB	50,000	0.193	4

amplitude of the frame acceleration, since this frequency range corresponds to the seat quasi-static and resonance zones. Low frequency modes are excited by the soil irregularity; as shown in Fig. 21, the PSD of the soil presents in fact relevant components in three frequency ranges (PSD is plotted against the ratio between forward speed and spatial wavelength): 0–2 Hz, 7–9 Hz, 16–17 Hz. High frequency excitation is filtered out by the suspensions, but low frequency contributions, associated with grooves due to previous plowings, are able to excite the rigid motions of seat and cabin.

Fig. 22 displays the spectra of seat acceleration in the range 0–5 Hz considering the four possible combination of tire and terrain. The terrain stiffness is able to affect the contribution of the heave and pitch modes; higher peak amplitudes occur on the harder soil. Considering the same soil, the larger tire gives rise to the higher acceleration components. Data of Table 5 can explain this result: a softer soil coupled with a narrower tire results in a lower contact stiffness. It should also be noticed how, a deeper sinking in the terrain implies higher energy dissipation due to the non-elastic response of the soil and to frictional forces exchanged by the tread; this mechanism can provide a further damping effect.

5. Front suspensions influence

During machinery operations, the front suspensions of a tractor are usually locked to maintain a greater control over pitch angle, which implies better results during tillage [12]. Despite this, the suspensions can be unlocked in order to improve driver comfort while running on ordinary roads or during driving on agricultural soil. Starting from the optimal values of damping of cabin and seat suspensions resulting from the previous analysis, effect of damping of front suspensions on comfort levels was investigated. On the basis of the frequency response shown in Figs. 2–5, unlocking front suspensions allows a significant reduction of the peaks associated with rigid motions of the cabin. In particular, the comparison between Figs. 2 and 3 with Figs. 4 and 5 evidences a reduction of the peaks associated with cabin pitch and heave due to the damping introduced by the front suspension.

Fig. 23 shows the standard deviation of seat vertical acceleration as a function of the damping value set for front suspensions. Numerical results point out that, if a proper damping level is provided, unlocking front suspension can bring to a further improvement of comfort levels.

Table 7 lists the values of RMS of vertical acceleration on the driver seat achievable with the optimal value of front suspension damping. The last column of Table 7 is

relevant to the improvements with respect to the values of Table 6 (i.e. optimal configuration with front suspension locked).

Recalling the data of Table 2, the nominal value for the damping of front suspensions is 40,000 Ns/m; the nominal value of damping for the front suspension appears suitably tuned for the considered vehicle, being in fact halfway between the optimal values found for harder and soft terrain. The examination of Table 7 shows that unlocking front suspension could lead to further improvement of comfort levels, especially on the stiffer terrain. Again, since comfort is mainly affected by low frequency components of vertical acceleration, the effect of tread design and tire type is limited.

6. Conclusion

This paper presented a numerical investigation of the role played by suspension parameters, tire characteristics and terrain response on the comfort levels of an agricultural tractor.

A 3D multi-body model of a tractor was developed and its parameters were identified though comparison with experimental data collected during tests on a 4-poster full scale test bench. The model of the tractor was interfaced with a tire–terrain interaction model; this last is able to take into account the 3D geometry of the tread and to describe the interaction between the tire and the deformable soil. Numerical simulations were carried out considering a tractor moving at constant speed on two different soils with two different sets of tires. Vertical acceleration on the driver seat was then estimated considering different tunings of front axle, cabin and seat suspension.

Numerical results showed that acceleration on the driver seat is characterized mainly by components below 5 Hz due to the rigid motions of the cabin and the seat itself. This means that the suspension system is effective in filtering out the higher harmonic components associated with terrain irregularity and tread lugs. Factors like lugs number and height, thus give a minor contribution to the overall seat acceleration.

By contrast, suspensions tuning plays a significant role in affecting comfort levels; in particular, as far as the examined vehicle is concerned, a proper setting of cabin and seat damping would allow a reduction of the acceleration levels on driver seat between 20% and 30% with respect to the nominal configuration, depending on terrain properties. Unlocking the front suspensions, when possible, leads to a further reduction between 5% and 10%.

Rigid motions of seat and cabin are excited by the soil undulation due for example to previous tillage operations or passage of other vehicles. The terrain PSD in a wavelength range between 1 and 10 m thus plays an important role as excitation source.

Another important factor is represented by soil mechanical properties: the equivalent vertical stiffness displayed by the terrains considered in this work is comparable to the radial stiffness of the tires equipping the tractor. Deformation of tire and ground provides in fact another suspension level; running on the softer terrain produced acceleration levels 15–20% lower with respect to the harder one. It should be also pointed out that a deeper sinking of the tire in the terrain emphasizes the mechanisms of energy dissipation associated with terrain plasticity and frictional forces exchanged at the contact interface. This can provide an additional explanation for the improved comfort levels predicted for the softer terrain.

References

[1] Nguyen VN, Inaba S. Effects of tire inflation pressure and tractor velocity on dynamic wheel load and rear axle vibrations. J Terr 2011;47:3–16.

[2] Milosavljevic S, McBride DI, Bagheri N, Vasiljev RM, Mani R, Carman AB, et al. Exposure to whole-body vibration and mechanical shock: a field study of quad bike use in agriculture. Ann Occup Hyg 2011;55(3):286–95.

[3] Olson R, Hahn DI, Buckert A. Predictors of severe trunk postures among short-haul truck drivers during non-driving task: an exploratory investigation involving video assessment and driver behavioural self-monitoring. Ergonomics 2009;52(6):707–22.

[4] Anthonis J, Deprez K, Moshouu D, Ramon H. Design and evaluation of a low-power mobile shaker for vibration tests on heavy wheeled vehicles. J Terr 2000;37(4):191–205.

[5] International Organization for Standardization. Mechanical variation and Shock-evaluation of Human Exposure to Whole Body Vibration, part 1: General requirements. ISO 2631/1 1997.

[6] Servadio P, Marsili A, Belfiore NP. Analysis of driving seat vibration in high forward speed tractors. Biosystem Eng 2007;97:171–80.

[7] Braghin F, Genoese A, Sabbioni E, Bisaglia C, Cutini C. Experimental evaluation of different suspension systems for agricultural vehicles through four-poster test bench. In: Proceedings of 11th VSDIA conference Budapest, Hungary: 2008.

[8] Braghin F, Genoese A, Sabbioni E, Bisaglia C, Cutini C. Experimental modal analysis and numerical modeling of agricultural vehicles. Conference and exposition on structural dynamics (IMAC XXVII). Florida: Orlando; 2009.

[9] Wong JY. Terramechanics and off-road vehicle engineering. Oxford, United Kingdom: Butterworth-Heinemann; 2010.

[10] Braghin F, Cheli F, Melzi S, Negrini S, Sabbioni E. Experimental modal analysis and modelling of an agricultural tire. In: Proceedings of 13th VSDIA conference Budapest, Hungary: 2012.

[11] Muro T, O'Brien J. Terramechanics: land locomotion mechanics. Lisse, The Netherlands: AA Balkema Publishers; 2004.

[12] Braghin F, Cheli F, Colombo M, Sabbioni E, Bisaglia C, Cutini M. Characterization of the vertical dynamic behaviour of an agricultural vehicle. Proceedings of the ECCOMAS thematic conference in multibody dynamics. Italy: Milan; 2007.